PAPER

Tuning the magnetic anisotropy of Co–Ni nanowires: comparison between single nanowires and nanowire arrays in hard-anodic aluminum oxide membranes

To cite this article: V Vega *et al* 2012 *Nanotechnology* **23** 465709

Nanotechnology **23** (2012) 465709 (10pp) doi:10.1088/0957-4484/23/46/465709

Tuning the magnetic anisotropy of Co–Ni nanowires: comparison between single nanowires and nanowire arrays in hard-anodic aluminum oxide membranes

V Vega[1], T Böhnert[2], S Martens[2], M Waleczek[2], J M Montero-Moreno[2], D Görlitz[2], V M Prida[1] and K Nielsch[2]

[1] Departamento Física, Universidad de Oviedo, Calvo Sotelo s/n, E-33007-Oviedo, Spain
[2] Institute of Applied Physics, University of Hamburg, Jungiusstraße 11, D-20355 Hamburg, Germany

E-mail: vegavictor@uniovi.es

Received 11 July 2012, in final form 16 September 2012
Published 24 October 2012
Online at stacks.iop.org/Nano/23/465709

Abstract
Co_xNi_{1-x} alloy nanowires with varying Co content ($0 \leq x \leq 0.95$), having a diameter of 130 nm and length of around 20 μm, are synthesized by template-assisted electrodeposition into the nanopores of SiO_2 conformal coated hard-anodic aluminum oxide membranes. The magneto-structural properties of both single isolated nanowires and hexagonally ordered nanowire arrays of Co–Ni alloys are systematically studied by means of magneto-optical Kerr effect magnetometry and vibrating sample magnetometry, respectively, allowing us to compare different alloy compositions and to distinguish between the magnetostatic and magnetocrystalline contributions to the effective magnetic anisotropy for each system. The excellent tunable soft magnetic properties and magnetic bistability exhibited by low Co content Co–Ni nanowires indicate that they might become the material of choice for the development of nanostructured magnetic systems and devices as an alternative to Fe–Ni alloy based systems, being chemically more robust. Furthermore, Co contents higher than 51 at.% allow us to modify the magnetic behavior of Co-rich nanowires by developing well controlled magnetocrystalline anisotropy, which is desirable for data storage applications.

(Some figures may appear in colour only in the online journal)

1. Introduction

The synthesis of nanostructured materials by means of electrochemical deposition into the pores of nanoporous anodic aluminum oxide (AAO) membranes has attracted a huge scientific interest due to the outstanding features exhibited by these templates such as low cost, large self-ordering degree of the nanopores, high reproducibility and precise control over their morphological characteristics [1]. In the last years, AAO membranes have been used as templates for the synthesis of a large variety of nanomaterials comprising nanowires [2–4], nanotubes [5, 6], dots [7] and antidots [8, 9] made of several materials of technological interest, for instance noble metals, ferromagnetic materials and alloys, or thermoelectrics and semiconductors [10].

Recently, the peculiar characteristics of hard-anodic aluminum oxide (H-AAO) membranes, mainly the low processing time, large interpore distance, and a broad window of self-ordering conditions [11], have been demonstrated to be advantageous for their use as templates in the fabrication of highly-ordered nanowire arrays. The high nanoporous oxide growth rate achieved by means of this method (about 50 μm h^{-1}, 20 times faster than standard mild anodization), together with the fast development of a hexagonal highly-ordered nanoporous arrangement, allow us to produce H-AAO membranes with reproducible geometrical parameters in a few hours by only performing a single

anodization step [11]. It is worth noting that this single-step anodization approach is especially suitable for AAO membranes grown under hard anodization (HA) conditions, but it is not appropriate when combined with standard mild anodization (MA). The nanopore ordering process during MA is slow and therefore it implies the development of a thicker and disordered nanoporous alumina film on the top surface of the AAO membrane that is not suitable for its use as a template, therefore resulting in a reduced throughput of this nanofabrication technique.

Although the HA fabrication process is very promising, limited work has been published up to now displaying applications of H-AAO membranes employed as templates for the synthesis of nanostructured materials in a systematic way [12–15].

Co–Ni alloy nanowires are outstanding magnetic materials that can exhibit either a soft or a hard magnetic behavior depending on the Co content in the alloy [16, 17]. The combination of low magnetocrystalline anisotropy of face centered cubic (fcc) Ni and high magnetocrystalline anisotropy of hexagonal close-packed (hcp) Co, together with the high solubility of Co atoms in the crystalline lattice of Ni, and vice versa, for a wide range of relative concentrations [18], allows for the design of a material composition with tunable magnetic properties. The room temperature (RT) uniaxial magnetocrystalline anisotropy constant of bulk Co–Ni alloys, K_1, can vary from negative values (-5×10^4 erg cm^{-3}) for pure Ni to positive ones (2×10^4 erg cm^{-3}) with the addition of a moderate amount of Co (8–22 Co at.%), whereas higher Co contents result in larger negative values (-2×10^5 erg cm^{-3}) [19]. Therefore it is possible to select a particular composition in the Ni-rich range showing negligible magnetocrystalline anisotropy together with the softest magnetic properties.

In the case of densely-packed nanowire arrays, the effective anisotropy energy is determined by competition between shape and magnetocrystalline anisotropies, together with magnetostatic dipolar interactions among nanowires, it being possible to tune the preferred magnetization direction (easy magnetization axis) of the system between the longitudinal and perpendicular directions with respect to the nanowires axis [20, 21]. Consequently, accurate control of the crystalline anisotropy plays a key role in the design of nanostructured magnetic materials with a required magnetic behavior, suitable for applications in diverse fields of technological interest such as magnetic devices with memory effect and electromagnetic pulse detection systems [22], racetrack memory devices with tailored pinning centers for domain wall propagation [23] and stable domain wall velocity [24], or selective cell manipulation [25].

In the present work, highly hexagonally ordered H-AAO membranes have been used as templates for the synthesis of potentiostatically electrodeposited Co–Ni nanowire arrays covering a wide range of compositions from pure Ni to $Co_{0.95}Ni_{0.05}$, demonstrating the huge potential of such patterned templates for the synthesis of self-assembled nanomaterials. A thin layer of SiO_2 conformal coating is deposited by atomic layer deposition on the surface of H-AAO templates as a protective outer shell that covers the nanowires, avoiding their oxidation, allowing us to release them from the H-AAO template by selective chemical etching without any damage and to study the magnetic behavior of non-interacting single nanowires by means of spatially resolved magneto-optical Kerr effect (MOKE) magnetometry. We have systematically analyzed the main contributions to the effective magnetic anisotropy for the different compositions and crystalline phases of the Co–Ni nanowire arrays. Our results indicate that low Co content Co_xNi_{1-x} nanowires ($0 \leq x \leq 0.51$) exhibit a tunable coercivity (ranging from 200 up to 400 Oe) while maintaining a bistable magnetic behavior. However, higher Co content nanowires ($x \geq 0.71$) reveal an increasing magnetocrystalline anisotropy that competes against the magnetostatic one, breaking down their magnetic bistability. Therefore, Co–Ni alloys could become a good alternative to Fe–Ni alloys with some specific advantages, such as the possibility of inducing tunable magnetocrystalline anisotropy by carefully controlling their composition, giving additional degrees of freedom for tailoring the magnetic and magneto-transport [26–29] behavior of nanostructured systems and devices. For instance, high anisotropic magnetoresistance values of about 20% have been recently reported in electrodeposited Co–Ni thin films [30].

2. Experimental section

2.1. Synthesis of H-AAO templates

High purity aluminum foils (Goodfellow, Al 99.999%) were first cleaned by means of ultrasonication in isopropanol and ethanol for 5 min. Afterwards, the Al foils were placed into an anodization cell and electropolished up to a mirror-like finish in a vigorously stirred mixture of perchloric acid and ethanol (25:75 vol.%) at 5 °C, with an applied voltage of 20 V measured versus a Pt counter-electrode. H-AAO membranes were synthesized by a single anodization step performed at 140 V for 1.5 h in a 0.3 M oxalic acid aqueous solution containing 5 vol.% of ethanol at a temperature between 0 and 3 °C. Before the HA process, the Al substrates were pre-anodized under mild anodization conditions at 80 V for 10 min and then the anodization voltage was increased at 0.08 V s^{-1} to reach potentiostatic conditions in the HA process. The characteristic current transient obtained during the pre-anodization (I), voltage ramp (II) and HA processes (III), respectively, is shown in figure 1(a). During the voltage ramp (stage II) the anodization current density, j_{an}, exponentially increases with the increment of anodization voltage. At a certain value of the anodization voltage, close to 100 V, j_{an} displays a local maximum that can be associated with the beginning of the HA regime. Once the final HA voltage of stage III is reached, j_{an} shows a fast decrease as a function of the anodization time, which is ascribed to the increased diffusion path of the electrolyte anions involved in the anodization reaction [11]. After the HA process, the un-oxidized Al substrate was removed by wet chemical etching in a $CuCl_2$/HCl aqueous solution and the

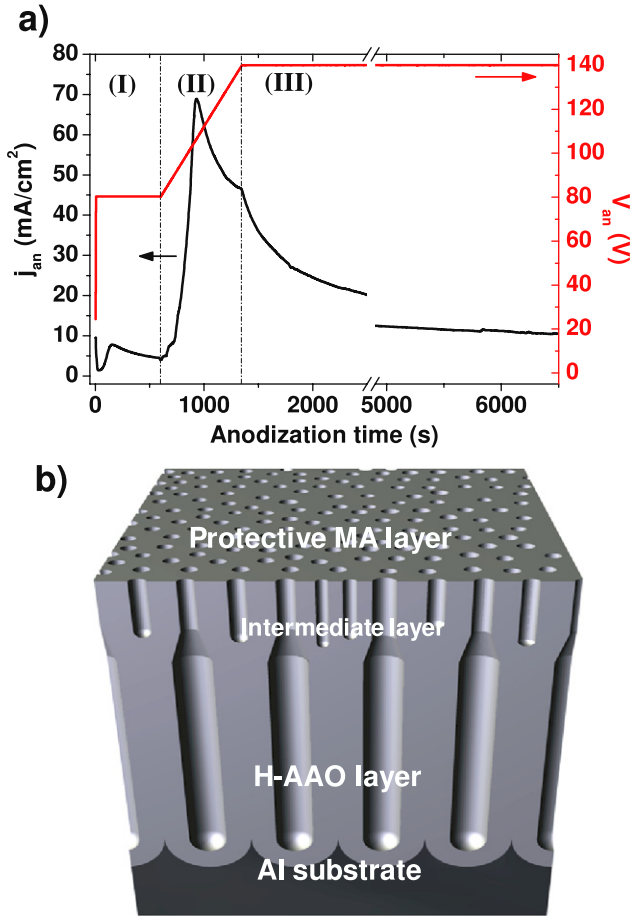

Figure 1. (a) Current transients during the pre-anodization (I), voltage ramp (II) and HA (III) stages. (b) Schematic drawing of a typical H-AAO membrane.

membranes were subsequently immersed for 2.5 h in 5 wt.% H_3PO_4 at 30 °C in order to remove the alumina barrier layer at the bottom of the pores, also increasing the pore size of the H-AAO membranes. This last chemical etching step also results in a complete dissolution of the protective mild anodization AAO layer on top of the H-AAO membranes, due to its lower chemical resistance to phosphoric acid etching compared to the H-AAO layer. Therefore the pores of the resulting H-AAO membrane are fully opened at both sides. Afterwards, the membranes were coated with a protective SiO_2 conformal layer of thickness 10 nm, deposited by atomic layer deposition at 150 °C from aminopropyltriethoxysilane (100 °C), water (RT) and ozone (RT) employed as precursors and oxidizing agent, respectively [31]. The back side of the H-AAO templates was coated by means of sputtering and further electrodeposition of a continuous gold layer, which serves as working electrode in the subsequent Co–Ni electrodeposition process.

2.2. Electrodeposition of Co–Ni nanowire arrays

Nanowire arrays of the Co_xNi_{1-x} alloys ($0 \leq x \leq 0.95$) were electrochemically grown from Watts-type baths containing different amounts of Co^{2+} ions, ranging from 0% to 64.5%, as specified in table 1. The pH of the electrolytes was adjusted to a value of 4–4.2 by adding 1 M NaOH. Electrodeposition processes were carried out at 35 °C under potentiostatic conditions in a three-electrode electrochemical cell equipped with a KCl 3M Ag/AgCl reference electrode, an insoluble Pt mesh counter-electrode and the gold coated H-AAO template acting as the working electrode. The net charge flowing through the electrochemical cell was controlled *in situ* and it was kept at 2.19 mA h cm^{-2}, resulting in the growth of high aspect ratio Co–Ni nanowires of about 15–30 μm in length. The composition of the Co_xNi_{1-x} nanowire arrays ($0 \leq x \leq 0.95$) was adjusted either by varying the electrolyte composition or by adjusting the deposition potential between −0.8 and −1.0 V versus the reference electrode. After the Co–Ni electrodeposition process, gold caps of about 2 μm in length were deposited in the upper part of the nanowires to protect them from corrosion.

Table 1. Watts-type electrochemical baths employed for the potentiostatic electrodeposition of Co–Ni nanowire arrays.

$CoSO_4$ (mol l^{-1})	$CoCl_2$ (mol l^{-1})	$NiSO_4$ (mol l^{-1})	$NiCl_2$ (mol l^{-1})	H_3BO_3 (mol l^{-1})	Co^{2+} molar ratio (%)
0.71	0.09	0.38	0.06	0.73	64.5
0.53	0.06	0.57	0.11	0.73	46.9
0.36	0.04	0.76	0.13	0.73	30.7
0.18	0.02	0.95	0.16	0.73	15.2
0.11	0.01	1.14	0.21	0.73	8.1

2.3. Preparation for single wire MOKE measurements

In order to perform a systematic study of the magnetic properties of single isolated Co–Ni nanowires, it was necessary to release them from the H-AAO template via a chemical etching procedure. Firstly, the gold layer was partially removed by wet chemical etching in KI 0.6 M and I_2 0.1 M aqueous solution, and the SiO_2 protective coating covering the empty parts of the H-AAO template was removed by dipping the sample in diluted HF. Afterwards, the alumina membrane, which contains embedded the nanowire arrays, was immersed in a mixture of H_3PO_4 (6 wt.%) and CrO_3 (1.8 wt.%) at 45 °C for 48 h, resulting in the total dissolution of the alumina template. Free-standing nanowires, protected by a thin and transparent SiO_2 coating and gold caps in both extremities of the nanowires, were then filtered and suspended in absolute ethanol. For single nanowire characterization, a drop of the nanowire suspension was deposited on a Si wafer and dried with a nitrogen stream.

2.4. Measurement methods

The microstructure and chemical composition of the samples was studied by scanning electron microscopy (SEM, Supra 55-Zeiss) and energy dispersive x-ray microanalysis (EDX). X-ray diffraction (XRD, X'Pert PRO-PANalytical) patterns were acquired in a θ–2θ setup by employing Cu $K_{\alpha 1}$ radiation ($\lambda = 1.540\,56$ Å), in order to determine the crystalline phases present in the Co_xNi_{1-x} nanowire arrays with varying

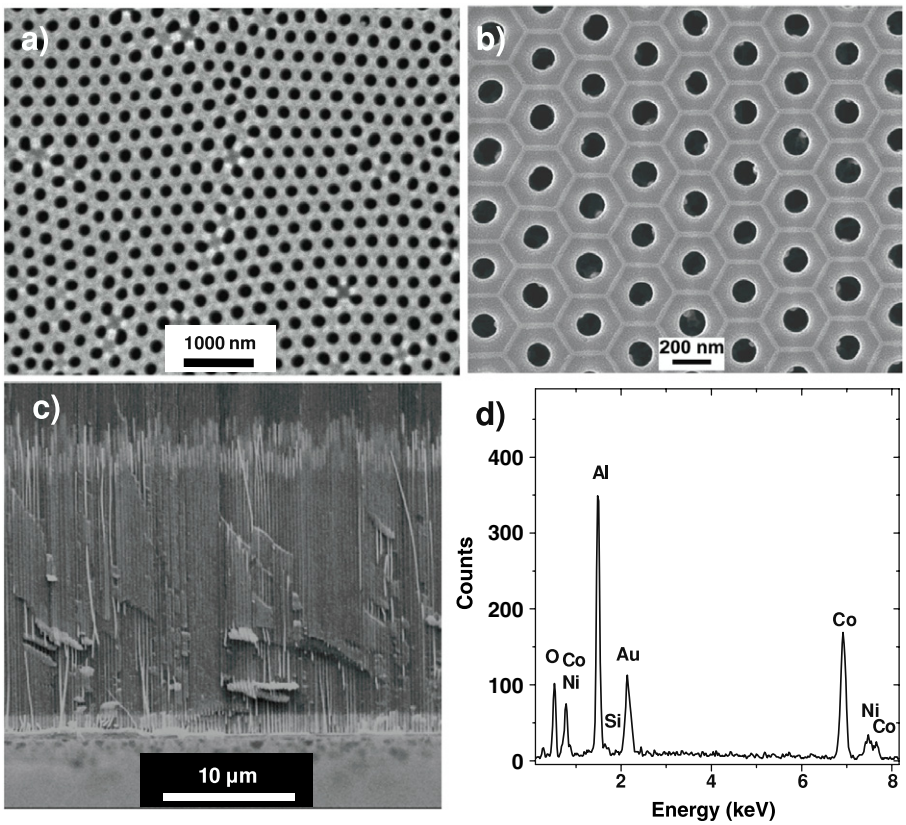

Figure 2. (a) SEM bottom view of a SiO_2 coated H-AAO membrane used as template for Co–Ni nanowire arrays synthesis. (b) High magnification SEM picture of the image shown in (a), displaying the short range hexagonal ordering of the pores. (c) SEM cross-sectional view of Co–Ni nanowires grown into the nanoporous template. (d) EDX spectrum obtained from the SEM cross-sectional view.

composition ($0 \leq x \leq 0.95$). The magnetic properties of arrays of Co–Ni nanowires were studied at RT as a function of the Co content by means of a vibrating sample magnetometer (VSM, Versalab-Quantum Design), with a maximum range of the applied magnetic field of ±30 kOe. The hysteresis loops of single isolated nanowires were measured in a MOKE magnetometer (NanoMOKE2-Durham Magneto Optics) at RT by employing a polarized laser beam with a spot size of about 3 μm and under a maximum magnetic field value of ±600 Oe, applied parallel to the nanowire axis and the deflection plane, i.e. utilizing the longitudinal Kerr effect. The drawbacks of the low signal to noise ratio in the MOKE for measuring the magnetic behavior of nanostructures were overcome by averaging several hundred single-shot measurements. The coercive fields of single wires are obtained as the most prevalent coercive field value from the statistical analysis of the coercivity of 100 different single wires of the same composition and morphology, and some arbitrary selected hysteresis loops are shown as examples. This technique has been recently demonstrated to be a powerful tool for studying the magnetic behavior of single cylindrical nanostructures [32]. Although the MOKE signal is generally related to the surface magnetic structure of bulk materials [33], in our case the penetration depth of the laser beam has been estimated to be about 20–30 nm for Co–Ni alloy nanowires, which is large enough to consider that this volume fraction of the sample is representative of the whole magnetization signal of a nanowire.

The SiO_2 shell causes a Faraday contribution to the MOKE signal, which is independent of the applied field and thus has no influence on the recorded magneto-optic hysteresis loops.

3. Results and discussion

3.1. Morphological, compositional and structural characterization

H-AAO templates, produced in a single anodization step as described in section 2, are schematized in figure 1(b). Three different layers can be distinguished, namely, a protective MA top layer, an intermediate AAO layer where pore re-arrangement occurs due to a change from MA to HA conditions and, finally, the highly-ordered H-AAO layer in contact with the Al substrate. Figure 2(a) shows a scanning electron microscope (SEM) image of the bottom surface of a typical H-AAO layer used for the synthesis of Co–Ni nanowire arrays after detaching it from the Al substrate and submitting it to a pore-widening process, where the existence of polydomain porous structures displaying a high hexagonally ordering can be observed. Figure 2(b) is a higher magnification SEM picture of figure 2(a), displaying the short range hexagonal ordering of the pores achieved

during the HA processes. The interpore distances and pore diameters of the H-AAO have been estimated to be about 305 and 150 nm, respectively. In order to protect the isolated Co–Ni nanowires from oxidation after removing the alumina template by chemical etching, the H-AAO membranes were previously coated with a 10 nm thick conformal SiO_2 layer that was deposited by atomic layer deposition [31], resulting also in a reduction of the pore diameter to about 130 nm, giving an estimated membrane packing factor, P, of about 16%, as calculated following [34].

This unique template-based strategy that combines the self-ordered nanopore arrangement of H-AAO membranes together with the protective SiO_2 conformal coating deposited by atomic layer deposition allows the design of engineered patterned templates for the synthesis of both ordered arrays of nanowires and isolated wires after selective chemical etching.

Pore filling of these novel patterned templates was performed by electrochemical deposition of Co–Ni alloys with controlled composition from Watts-type baths under potentiostatic conditions. Figure 2(c) shows a SEM image of a cross-sectional view of $Co_{0.64}Ni_{0.36}$ nanowires about 20 μm long embedded in a H-AAO template. The compositional contrast observed in the SEM image also indicates the presence of gold caps at the top and bottom of the nanowires that were electrochemically deposited in order to protect the Co–Ni nanowire arrays from corrosion.

The chemical composition of the Co–Ni nanowire arrays was determined by analyzing the EDX spectra obtained from cross-sectional SEM studies. As an example, one of these EDX spectra is shown in figure 2(d), in which the presence of both elements, Co and Ni, together with Al, O and Si coming from the SiO_2 coated H-AAO template can be observed. The influence of both the Co^{2+} ion ratio in the electrolyte and the electrodeposition potential value employed on the final composition of the Co–Ni alloy is depicted in figure 3(a). Although the standard reduction potential of Ni ($E^0 = -0.26$ V) is higher than that of Co ($E^0 = -0.28$ V), and therefore Ni is electrochemically more noble than Co, it can be seen that even at low Co^{2+} ion concentrations in the electrolyte, high cobalt contents were found in the corresponding nanowire arrays. For example, nanowires grown at -1 V from the electrolyte containing about 30 at.% of Co^{2+} ions have a Co content higher than 70 at.%. This effect becomes even more noticeable at lower electrodeposition potentials. This phenomenon, which is known as anomalous co-deposition of Co, has been tentatively explained in terms of the hydroxide suppression mechanism [35, 36] or ascribed to the inhibition of Ni deposition due to adsorbed Co^{2+} ions [37]. By taking advantage of the above mentioned electrochemical behavior for Co–Ni alloy electrodeposition, it has been made possible to tune the composition of the Co–Ni nanowire arrays either by varying the electrolyte composition or by adjusting the deposition potential.

The XRD measurements performed in a θ–2θ configuration in some relevant Co–Ni alloy nanowire arrays are shown in figure 3(b). It can be observed that Ni-rich samples ($Co_{0.23}Ni_{0.77}$ and $Co_{0.38}Ni_{0.62}$) exhibit a fcc structure typical

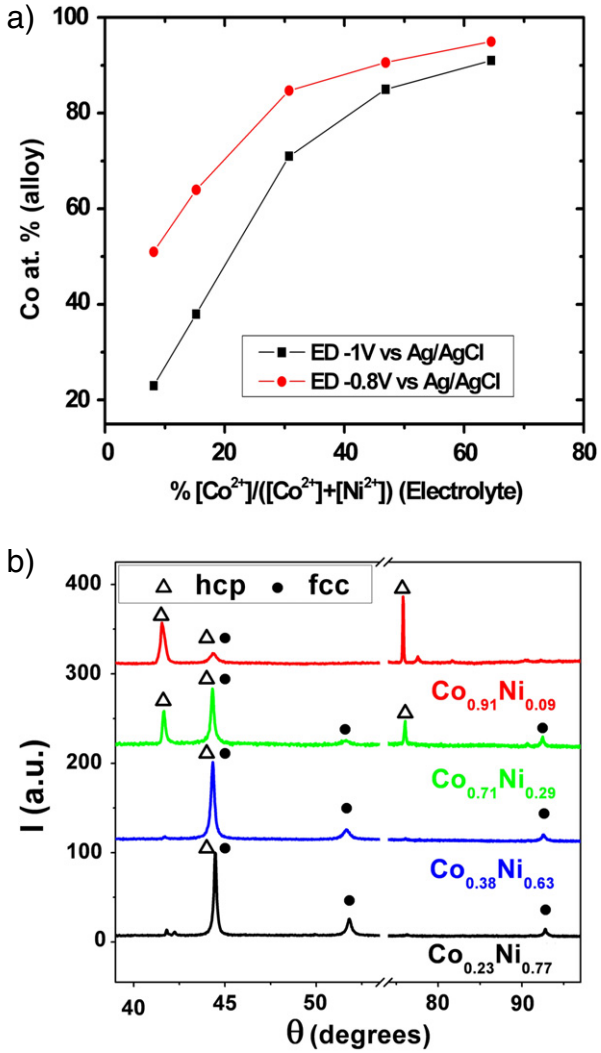

Figure 3. (a) Dependence of the Co content in the Co–Ni nanowire arrays on the Co^{2+} ion ratio in the electrolyte at different electrodeposition potentials. (b) XRD data for Co_xNi_{1-x} nanowire arrays with different Co contents ($0.23 \leq x \leq 0.91$).

for Ni, in which Ni atoms are partially substituted by Co. This crystalline phase tends to disappear as the Co content of the nanowires increases, due to the development of a hcp crystalline phase, characteristic of pure Co. In the case of $Co_{0.71}Ni_{0.29}$ nanowire arrays, both fcc and hcp phases coexist, while for $Co_{0.91}Ni_{0.09}$ nanowire arrays the fcc phase has totally disappeared, suggesting that Ni partially replaces Co atoms in the hcp lattice. The average crystallite size has been evaluated from line width analysis of XRD spectra by using the Scherrer equation, resulting in values of 5 ± 2 nm for fcc crystals and 9 ± 2 nm for hcp ones, thus evidencing the polycrystalline structure of the nanowires.

3.2. Magnetic characterization

Co–Ni nanowire arrays show a broad spectrum of magnetic behaviors depending on the relative amount of Co contained in the alloy. Figure 4 (left column) shows normalized RT VSM magnetic hysteresis loops of Co–Ni nanowire arrays

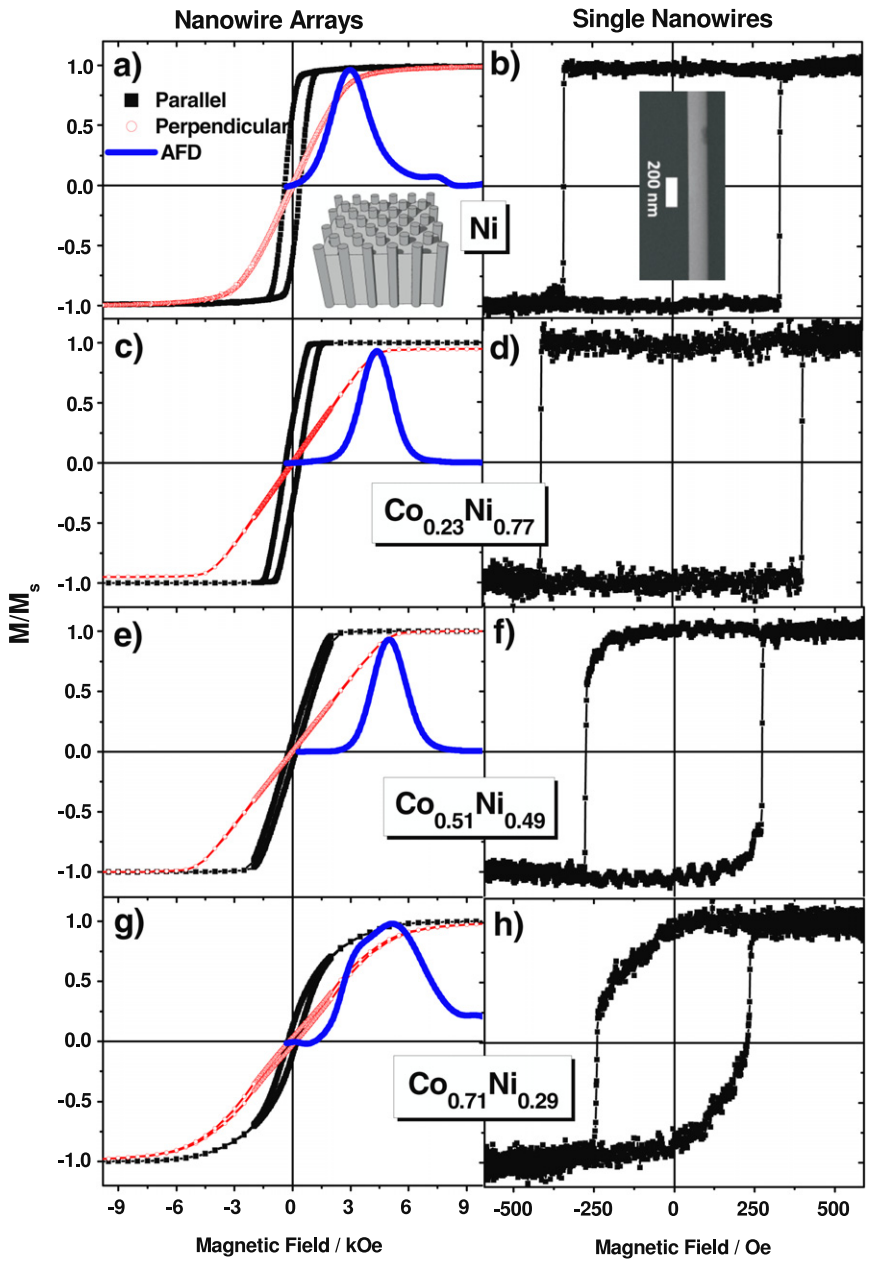

Figure 4. Normalized hysteresis loops of selected Co–Ni nanowire arrays and single nanowires, with different compositions ranging from pure Ni to $Co_{0.71}Ni_{0.29}$. Left column: VSM hysteresis loops of Co–Ni nanowire arrays measured along the directions parallel and perpendicular to the nanowires axis, together with the AFD curve obtained from perpendicular hysteresis loops. Right column: some examples of the MOKE parallel hysteresis loops measured for single Co–Ni nanowires with the same compositions. The insets in graphs (a) and (b) display a sketch of a hexagonally ordered array of nanowires and a SEM image of a single nanowire, respectively.

with Co contents ranging from 0 up to 71 at.%, measured in both parallel and perpendicular directions with respect to the longitudinal axis of the nanowires, together with the anisotropy field distribution (AFD) curves calculated for each composition of Co–Ni nanowire arrays. AFD curves ($\sigma(H_A)$) have been obtained from the numerical derivative of the descent from positive saturation of the magnetization branch, down to remanence, of the perpendicular hysteresis loop of nanowire arrays, according to equation (1) [38]

$$\sigma(H_A) = -H\frac{d^2}{dH^2}\langle M(H)\rangle\bigg|_{H=H_A}. \qquad (1)$$

This method, developed by Barandiaran *et al* [39] and successfully adapted to the study of magnetic nanowires by de La Torre Medina *et al* [38], provides a simple approach to determine the most prevalent value of the anisotropy field (H_A) of a magnetic material. This value can be directly related to the effective anisotropy field, which is the field necessary to saturate the material along the magnetization hard axis, when certain conditions regarding the size and geometry of the material, together with a low magnetocrystalline anisotropy, are fulfilled [38].

Figure 4 (right column) presents some arbitrarily selected examples of RT MOKE hysteresis loops measured along

the axis of single nanowires with the same composition as for the corresponding arrays of nanowires (on the left). A substantially different magnetic behavior can be observed when comparing the Ni-rich and Co-rich Co–Ni single nanowires and nanowire arrays.

3.2.1. Ni-rich Co–Ni nanowires. The ferromagnetic behavior of Ni-rich Co_xNi_{1-x} alloy nanowires, with x ranging between 0 and 0.51, is mainly governed by the predominance of shape magnetic anisotropy, since the magnetocrystalline anisotropy nearly vanishes at RT for these alloy compositions, indicating that Co–Ni alloys can display excellent soft magnetic properties that may turn them into a good alternative to other soft magnetic alloys such as Ni–Fe [40]. The easy magnetization axis lies along the longitudinal axis of the nanowires (parallel direction), while the hard one remains in the plane perpendicular to the nanowires axis (perpendicular direction). The nanowire arrays show relatively high coercivity values for the parallel direction, $H_{c\parallel}$, ranging from 400 Oe for pure Ni down to about 200 Oe for $Co_{0.51}Ni_{0.49}$, whereas the squareness (M_R/M_S) values in the parallel direction, $m_{R\parallel} = M_{R\parallel}/M_S$, range between 60% (Ni nanowires) down to about 10% ($Co_{0.51}Ni_{0.49}$ nanowires). Such a decrease in the $m_{R\parallel}$ value as the Co content increases is related to the demagnetizing field, H_D, originating from the magnetostatic coupling among nanowires in the array, which is proportional to the saturation magnetization of the alloy and reaches its maximum value when the nanowires are all magnetized parallel with respect to their long axis [4, 41]. The increase of the saturation magnetization of Co–Ni alloys with the addition of Co atoms, as shown in the Slater–Pauling curve [42] and experimentally reported for bulk Co–Ni alloys [43–45], therefore causes an increase in the demagnetizing field which is responsible for the diminishing of the squareness value. By comparing the longitudinal VSM hysteresis loops of the Co–Ni nanowire arrays with the corresponding MOKE hysteresis loops of single isolated nanowires with the same composition, the influence of dipolar interactions among nanowires in the bulk of the array becomes even more evident. It can be seen that, for Ni, $Co_{0.23}Ni_{0.77}$ and $Co_{0.51}Ni_{0.49}$ compositions, MOKE hysteresis loops obtained from single nanowires are square in shape, having $m_{R\parallel}$ values close to 100%, pointing out the bistable magnetic behavior of these wires, where the magnetization reverses in a single Barkhausen jump. In contrast, the VSM hysteresis loops measured along the parallel direction for the corresponding nanowire arrays reveal that their easy magnetization axes are tilted out of the nanowire axis. This effect is due to both the switching field distribution of the nanowires and the influence of the demagnetizing field caused by the magnetostatic dipolar interactions among nanowires in the array. Such differences between the longitudinal hysteresis loops measured for single nanowires and nanowire arrays are in good agreement with both micromagnetic simulations performed by Zighem *et al* [46] and experimental measurements performed in similar systems of arrays of bistable magnetic microwires [47, 48], where it has been found that longitudinal hysteresis loops progressively tilt down when increasing the number of interacting wires in the array.

3.2.2. Co-rich Co–Ni nanowires. Co_xNi_{1-x} nanowires with high Co contents ($x \geq 0.60$) exhibit quite a different magnetic behavior. Hysteresis loops measured along the parallel direction to the wire axis have lost their squareness, suggesting a change in the magnetization reversal process, as can be seen from both the longitudinal hysteresis loop of $Co_{0.71}Ni_{0.29}$ nanowires array and the corresponding one for the single isolated nanowire. It is particularly clear that in the case of the isolated nanowire the magnetization does not fully reverse in a single Barkhausen jump. For example, when the applied magnetic field is reduced from positive saturation magnetization towards negative field values, the longitudinal component of the magnetization progressively decreases up to a threshold value at which it suddenly switches to the opposite magnetization state. This magnetic behavior is consistent with the above mentioned development of the hcp crystalline phase found in Co-rich Co–Ni nanowires. The higher value of the Co hcp crystalline anisotropy constant ($K_{hcp} = 4.1 \times 10^6$ erg cm^{-3}) than the corresponding one of the fcc structure ($K_{fcc} = 6.3 \times 10^5$ erg cm^{-3}) at RT [49], together with the polycrystalline nature of the nanowires, cause the existence of a broad distribution of magnetocrystalline anisotropy axes which is competing with the shape anisotropy of the nanowire ($K_{sh} \sim 6 \times 10^6$ erg cm^{-3}) [49], favoring local magnetization rotation processes. When the absolute value of the applied magnetic field reaches a value high enough to overcome the overall magnetic anisotropies, i.e. the effective magnetic anisotropy, the magnetization of the nanowire switches to its saturation value.

3.2.3. Comparison between Ni-rich and Co-rich Co–Ni nanowires. The coercivity dependence on the Co content of the alloy for both Co–Ni nanowire arrays and isolated nanowires, obtained respectively from VSM and MOKE hysteresis loops, is depicted in figure 5 (upper panel). In the composition range from pure Ni to $Co_{0.51}Ni_{0.49}$, the $H_{c\parallel}$ value monotonously decreases as the Co content increases for both single nanowires (from 404 to 241 Oe) and nanowire arrays (from 391 to 180 Oe), the one with $Co_{0.51}Ni_{0.49}$ composition exhibiting the softest magnetic properties. By directly comparing the values of $H_{c\parallel}$ for Co–Ni nanowire arrays with their respective counterparts for single isolated nanowires, obtained by taking the most prevalent value of the $H_{c\parallel}$ distribution from up to 100 different single wires with the same composition, it can be observed that the latter have larger values than the former for all the measured Co_xNi_{1-x} nanowires in the range of $0 \leq x \leq 0.62$, in good agreement with previous works [50], which demonstrates that the magnetostatic interactions among nanowires in the array are responsible for such a decrease in the coercivity. The coercive field values measured for nanowire arrays along the perpendicular direction to the nanowires axis ($H_{c\perp}$) show a small decrease from 71 to 44 Oe with increasing Co content in the same compositional range, whereas for higher Co contents it increases up to values of around 200 Oe, close to those of $H_{c\parallel}$, due to competition between shape and hcp magnetocrystalline anisotropies of Co-rich nanowires.

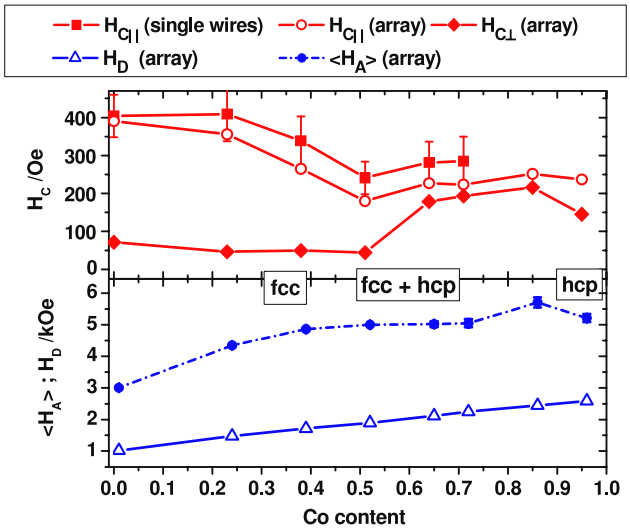

Figure 5. Coercivity (H_C) dependence on Co content for both Co–Ni nanowire arrays and single isolated nanowires (upper panel), together with the average anisotropy field ($\langle H_A \rangle$) and maximum dipolar interaction field (H_D) (lower panel). The error bars of the single wire MOKE measurements are obtained from the statistical evaluation of the coercivity of about 100 nanowires of each composition.

In order to clarify the contribution of the magnetocrystalline anisotropy to the magnetic behavior of Co–Ni nanowires, we have estimated the average anisotropy field, $\langle H_A \rangle$, taken as the field value at which the AFD curve (displayed in figure 4, left column) reaches its maximum [38]. The values of $\langle H_A \rangle$ are shown in figure 5 (lower panel), together with the maximum dipolar interaction field, H_D, calculated according to equation (2) and employing the saturation magnetization values, M_S, predicted by the Slater–Pauling curve [42] for each Co_xNi_{1-x} composition ($0 \leq x \leq 0.95$):

$$H_D = -4\pi P M_S \tag{2}$$

where P is the membrane packing factor mentioned earlier. It can be observed in figure 5 that for pure Ni, $\langle H_A \rangle$ reaches a value of 3.0 kOe, which increases up to 4.8 kOe in the compositional range of the alloy where a negligible magnetocrystalline anisotropy in Co_xNi_{1-x} nanowires ($0 \leq x \leq 0.38$) is expected. In this case, the $\langle H_A \rangle$ values can be directly related to the magnetostatic contributions to the effective anisotropy field [38], H_{ms} (shape anisotropy and dipolar interactions among wires in the array), and hence it will be given by equation (3)

$$\langle H_A \rangle = H_{ms} = 2\pi M_S(1 - 3P). \tag{3}$$

Thus, the increase in the $\langle H_A \rangle$ values is due to the increase in M_S as the Co content of the alloy varies from 0 up to 38 at.%.

It is worth noting that in the case of magnetic nanowires with non-negligible magnetocrystalline anisotropy, the interpretation of the relation between $\langle H_A \rangle$ and the effective magnetic anisotropy of the system is not straightforward, since it depends on the relative orientation of the magnetocrystalline anisotropy axes (c-axes in the case of hcp Co–Ni nanowires) with respect to the nanowire axis. On the one hand, if the c-axis lies perpendicular to the wires, the magnetocrystalline and magnetostatic anisotropies compete and $\langle H_A \rangle$ can be expressed as [38]

$$\langle H_A \rangle = H_{ms} - \tfrac{1}{2} H_{mc} \tag{4}$$

where H_{mc} is the magnetocrystalline anisotropy field. On the other hand, if the c-axis is parallel to the wires, both magnetostatic and magnetocrystalline terms add, and $\langle H_A \rangle$ is written as:

$$\langle H_A \rangle = H_{ms} + H_{mc}. \tag{5}$$

In more complex situations, where the c-axis orientation exhibits a certain angular distribution due to the polycrystalline structure of the nanowires, it becomes necessary to perform an average over their relative orientation.

These phenomena could explain the experimental deviation of the $\langle H_A \rangle$ curve from that predicted by equation (3) observed for nanowires with higher Co contents than 38 at.%. Instead of a monotonous increase of $\langle H_A \rangle$, a plateau in the range from 51 to 71 at.% Co is observed, which can be ascribed to the coexistence of both fcc and hcp crystalline phases, the latter having a higher magnetocrystalline anisotropy that counter-balances the magnetostatic contribution to the effective anisotropy. The competition established between magnetostatic and magnetocrystalline anisotropies is even more pronounced in Co_xNi_{1-x} alloys with higher Co contents than $x \geq 0.85$, where the hcp structure is the major crystalline phase. For these alloys, a slight modification of the electrochemical synthesis conditions can lead to significant changes in the direction of preferred growth of nanocrystals, and therefore it can be responsible for a sharp variation of the $\langle H_A \rangle$ or even cause a change of the preferred magnetization direction [20, 21, 38].

4. Conclusions

In conclusion, Co_xNi_{1-x} nanowire arrays with x ranging from 0 to 0.95 have been synthesized by means of template-assisted electrochemical deposition into the pores of SiO_2 conformal coated H-AAO membranes, demonstrating the suitability of employing such nanoporous templates for the synthesis of patterned nanostructures. Additionally, our fabrication procedure allows us to obtain single, non-interacting nanowires by releasing them from the alumina template. The cobalt content of the Co–Ni nanowires has been successfully tuned by varying both the Co^{2+}/Ni^{2+} ion ratio in the electrolyte and the applied electrodeposition voltage.

The magnetic characterization of both isolated Co–Ni nanowires and densely-packed Co–Ni nanowire arrays by means of MOKE and VSM techniques, respectively, allows us to differentiate between the inherent magnetic properties of single nanowires from those arising from the dipolar interactions among them. The dependence of the magnetic properties on the Co content has been systematically studied for both ordered arrays of nanowires and single isolated nanowires. The evolution from soft to hard magnetic behavior of Co–Ni nanowires has been ascribed to the change in the

crystalline structure of the nanowires that evolves from fcc for Ni-rich wires to hcp phase for Co-rich ones, together with the influence of the magnetostatic dipolar coupling among the nanowires in the array, which also varies proportionally to the M_S value for each Co_xNi_{1-x} composition ($0 \leq x \leq 0.95$).

Nanowires with a low Co content, Co_xNi_{1-x} ($0 \leq x \leq 0.51$), display outstanding soft magnetic properties mainly governed by shape anisotropy, exhibiting a tunable coercivity ranging from 200 up to 400 Oe. Nanowires with the composition $Co_{0.51}Ni_{0.49}$ show the lowest coercive field values for both isolated nanowires (241 Oe) and nanowire arrays (180 Oe), while keeping a bistable magnetic behavior that turns them into excellent candidates for the development of nanostructured soft magnetic materials with improved chemical robustness, as a remarkable alternative to Fe–Ni alloys.

In contrast, higher Co content nanowires ($x \geq 0.64$) develop an increasing magnetocrystalline anisotropy that competes against the magnetostatic one, breaking down the magnetic bistability. The tunable magnetocrystalline anisotropy of Co–Ni nanowires allows for either slight modification of the soft magnetic properties of the nanowires or domination of their overall magnetic behavior.

The combination of the unique magnetic properties exhibited by Co–Ni alloys together with the possibility of synthesizing tunable compositions of these nanowire arrays by means of careful control of the parameters of the electrochemical deposition process, allows for the development of advanced functional materials based on segmented nanostructures with suitable magnetic properties, which can play a relevant role in the design of novel spintronic devices.

Acknowledgments

The authors are grateful to R Zierold and L Akinsinde for their support with atomic layer deposition and SEM characterization, respectively. Financial support from EU-Nanomagma under FP7-214107-2, LEXI-Spintronic funded by the State of Hamburg and Spanish MICINN under MAT2009-13108-C02-01 and MAT2010-20798-C05-04 is acknowledged. VV acknowledges German Academic Exchange Service (DAAD) and University of Oviedo for the grants supporting his internships. Scientific support from the University of Oviedo SCTs is also recognized.

References

[1] Masuda H and Fukuda K 1995 *Science* **268** 1466
[2] Nielsch K, Müller F, Li A P and Gösele U 2000 *Adv. Mater.* **12** 582
[3] Vázquez M, Pirota K, Hernández-Vélez M, Prida V M, Navas D, Sanz R, Batallán F and Velázquez J 2004 *J. Appl. Phys.* **95** 6642
[4] Vega V, Prida V M, García J A and Vázquez M 2011 *Phys. Status Solidi* a **208** 553
[5] Inguanta R, Piazza S and Sunseri C 2008 *Electrochim. Acta* **53** 5766
[6] Zierold R, Wu Z, Biskupek J, Kaiser U, Bachmann J, Krill III C E and Nielsch K 2011 *Adv. Funct. Mater.* **21** 226
[7] Park S K, Noh J S, Chin W B and Sung D D 2007 *Curr. Appl. Phys.* **7** 180
[8] Navas D, Hernández-Vélez M, Vázquez M, Lee W and Nielsch K 2007 *Appl. Phys. Lett.* **90** 192501
[9] Béron F, Pirota K R, Vega V, Prida V M, Fernández A, Hernando B and Knobel M 2011 *New J. Phys.* **13** 013035
[10] Eftekhari A 2008 *Nanostructured Materials in Electrochemistry* (Weinheim: Wiley–VCH)
[11] Lee W, Ji R, Gösele U and Nielsch K 2006 *Nature Mater.* **5** 741
[12] Pitzschel K, Montero-Moreno J M, Escrig J, Albrecht O, Nielsch K and Bachmann J 2009 *ACS Nano* **3** 3463
[13] Lim J H, Rotaru A, Min S G, Malkinski L and Wiley J B 2010 *J. Mater. Chem.* **20** 9246
[14] Yang Z H, Li Z W and Kong L B 2010 *J. Alloys Compounds* **501** 173
[15] Santos A, Montero-Moreno J M, Bachmann J, Nielsch K, Formentín P, Ferré-Borrull J, Pallarès J and Marsal L F 2011 *ACS Appl. Mater. Interfaces* **3** 1925
[16] Talapatra S, Tang X, Padi M, Kim T, Vajtai R, Sastry G V S, Shma M, Deevi S C and Ajayan P M 2009 *J. Mater. Sci.* **44** 2271
[17] Vivas L G, Vázquez M, Escrig J, Allende S, Altbir D, Leitao D C and Araujo J P 2012 *Phys. Rev.* B **85** 035439
[18] Cheng S L and Huang C N 2008 *Synth. React. Inorg. M.* **38** 475
[19] Kadowaki S and Takahashi M 1975 *J. Phys. Soc. Japan* **38** 1612
[20] Vila L, Darques M, Encinas A, Ebels U, George J M, Faini G, Thiaville A and Piraux L 2009 *Phys. Rev.* B **79** 172410
[21] Pirota K R, Beron F, Zanchet D, Rocha T C R, Navas D, Torrejon J, Vázquez M and Knobel M 2011 *J. Appl. Phys.* **109** 083919
[22] Kou X, Fan X, Dumas R K, Lu Q, Zhang Y, Zhu H, Zhang X, Liu K and Xiao J Q 2011 *Adv. Mater.* **23** 1393
[23] Franchin M, Knittel A, Albert M, Chernyshenko D S, Fischbacher T, Prabhakar A and Fangohr H 2011 *Phys. Rev.* B **84** 094409
[24] Koyama T, Chiba D, Ueda K, Tanigawa H, Fukami S, Suzuki T, Ohshima N, Ishiwata N, Nakatani Y and Ono T 2011 *Appl. Phys. Lett.* **98** 192509
[25] Gao N, Wang H and Yang E H 2010 *Nanotechnology* **21** 105107
[26] Smit J 1951 *Physica* **16** 612
[27] Van Elst H C 1959 *Physica* **25** 708
[28] Berger L 1964 *Physica* **36** 1141
[29] Mcguire T R and Potter R I 1975 *IEEE Trans. Magn.* **11** 1018
[30] Tóth B G, Péter L, Révész Á, Pádár J and Bakonyi I 2010 *Eur. Phys. J.* B **75** 167
[31] Bachmann J, Zierold R, Chong Y T, Hauert R, Sturm C, Schmidt-Grund R, Rheinländer B, Grundmann M, Gösele U and Nielsch K 2008 *Angew. Chem.* **120** 6272
[32] Pitzschel K, Bachmann J, Martens S, Montero-Moreno J M, Kimling J, Meier G, Escrig J, Nielsch K and Görlitz D 2011 *J. Appl. Phys.* **109** 033907
[33] Chizhik A, Zhukov A, Blanco J M and Gonzalez J 2003 *J. Magn. Magn. Mater.* **254/255** 188
[34] Nielsch K, Choi J, Schwirn K, Wehrspohn R B and Gösele U 2002 *Nano Lett.* **2** 677
[35] Fan C and Piron D L 1996 *Electrochim. Acta* **41** 1713
[36] Tian L, Xu J and Qiang C 2011 *Appl. Surf. Sci.* **257** 4689
[37] Gómez E, Ramirez J and Vallés E 1998 *J. Appl. Electrochem.* **28** 71
[38] de La Torre Medina J, Darques M, Piraux L and Encinas A 2009 *J. Appl. Phys.* **105** 023909
[39] Barandiaran J M, Vázquez M, Hernando A, González J and Rivero G 1989 *IEEE Trans. Magn.* **25** 3330
[40] Shaker-Salem M, Sergelius P, Zierold R, Montero-Moreno J M, Görlitz D and Nielsch K 2012 *J. Mater. Chem.* **22** 8549

[41] Encinas-Oropesa A, Demand M, Piraux L, Huynen I and Ebels U 2001 *Phys. Rev.* B **63** 104415
[42] Bozorth R M 2003 *Ferromagnetism* (New Jersey: Wiley)
[43] Shih J W 1936 *Phys. Rev.* **50** 376
[44] Jiles D C, Chang T T, Hougen D R and Ranjan R 1988 *J. Phys. Colloq.* **49** 1937
[45] Kadowaki S and Takahashi M 1975 *J. Phys. Soc. Japan* **38** 1612
[46] Zighem F, Maurer T, Ott F and Chaboussant G 2011 *J. Appl. Phys.* **109** 013910
[47] Sampaio L C, Sinnecker E H C P, Cernicchiaro G R C, Knobel M, Vázquez M and Velázquez J 2000 *Phys. Rev.* B **61** 8976
[48] Knobel M, Sampaio L C, Sinnecker E H C P, Vargas P and Altbir D 2002 *J. Magn. Magn. Mater.* **249** 60
[49] Sánchez-Barriga J, Lucas M, Radu F, Martin E, Multigner Marin M P, Hernando A and Rivero G 2009 *Phys. Rev.* B **80** 184424
[50] Escrig J, Lavín R, Palma J L, Denardin J C, Altbir D, Cortés A and Gómez H 2008 *Nanotechnology* **19** 075713